MEASUREMENTS OF INJECTED BEAM DEFLECTIONS AT THE EXIT OF A CYCLOTRON INFLECTOR AS A FUNCTION OF APPLIED FIELD OR BEAM ENERGY PERTURBATIONS

M.P. DEHNEL, K.L. ERDMAN

Ebco Technologies Inc., 7851 Alderbridge Way, Richmond B.C., Canada V6X 2A4

L.ROOT, T.KUO

TRIUMF, 4004 Wesbrook Mall, Vancouver B.C., Canada V6T 2A3

Measurements of the central trajectories of 25 keV H^- beams at the exit of the EBCO/TRIUMF 1 MeV Test Cyclotron's spiral inflector have been made using quartz scintillators, a TV Camera, and image analysis equipment and software. Plots of the displacement of the central trajectories as a function of inflector electric potential, cyclotron magnetic field and beam injection energy changes are shown, and are compared to numerically computed data generated from an inflector design program. Details of the experimental methods, the hardware set-up and the results are reported.

1 Introduction

The TR series of cyclotrons (TR30, TR19, TR13) designed by TRIUMF and manufactured by Ebco Technologies Inc. utilize an external multi-cusp H^- ion source, an axial injection system and a tilted spiral inflector to inject the intense (up to 15 mA) high brightness beam into the centre region. The benefits of such a system are described elsewhere [1, 2, 3, 4].

It is important for the injection system and inflector to properly position the injected beam in the centre region for maximum beam transmission and minimal emittance growth [5]. The TR series of cyclotrons are well designed in this regard [6, 7, 8, 9]. However, fine tuning of the injected beam position is still required to maximize accelerated beam transmission. This is achieved by adjusting the following parameters: (a) the injection line steering magnet fields, (b) the beam injection energy, (c) the inflector electrode voltages, and (d) the cyclotron magnet field. Although it is a routine matter for a cyclotron operator to adjust these parameters for maximum beam transmission, the magnitude and direction of the beam's displacement at the inflector exit is not well known.

In this paper we describe beam displacements at the inflector exit of a 1 MeV test cyclotron as a function of changes in parameters (b) through (d), and comparisons with CASINO [10] models are made. It is hoped the information presented here will aid in centre region trouble-shooting, and provide a means for more informed injection tuning in future.

2 Experimental Set-Up

The beam measurements reported here were made using the EBCO/TRIUMF 1 MeV test cyclotron known as the CRM.

The CRM duplicates the center region of the TR series of cyclotrons out to the fifth turn [11]. The CRM is a completely functional cyclotron complete with many access ports and an ion source and injection system (ISIS) mounted on rails.

The injection axis is horizontal, and the cyclotron's acceleration plane is vertical. The ISIS equipment used for the experiments is as follows:

Ion Source: A TR19 type high brightness dc multicusp H^- ion source was used. It produces a mono-energetic 25 keV (nominal) beam with an output current of 2 mA contained within a normalized emittance of 0.24π mm·mrad in both phase planes. The beam is very stable and reproducible [12].

Injection Line: The injection line consists of a diagnostic box which houses horizontal/vertical steering magnets, a beamstop, vacuum pumps, a pinhole collimator mounted on a vacuum feedthru micrometer, and a series of ion-optical components as described in Table 1.

Table 1: The injection line's optical parameters.

Optical Parameter	Value
Initial System Drift	486 mm
Quad Rotation Angle	–21.7°
Quad Magnet 0 (field, length, bore)	0.278 kG, 95.9 mm, 50.0 mm
Drift	40.5 mm
Quad Magnet 1 (field, length, bore)	–0.490 kG, 93.1 mm, 50.0 mm
Drift	41.3 mm
Quad Magnet 2 (field, length, bore)	0.550 kG, 93.4 mm, 50.0 mm
Drift	40.6 mm
Quad Magnet 3 (field, length, bore)	–0.510 kG, 95.6 mm, 50.0 mm
Drift Space	20.5 mm
Axial Bore Field	0 kG (z = –140 mm),

Inflector: After exiting the quadrupole magnets the beam enters the axial bore and then the Belmont-Pabot type spiral inflector. The inflector entrance electrodes are rotated 14° clockwise from vertical. After the beam exits the inflector it travels in a dipole magnetic field which increases from 9.8 kG at the machine centre to 12.0 kG at a radius of 3.5 cm.

The bore field and the median plane dipole field in the vicinity if the inflector have been mapped and are known to within a few gauss. The inflector parameters as used for the CASINO calculations are listed in Table 2.

Table 2: The inflector parameters.

Parameter	Value
Electric bend radius	25 mm
Tilt: k'	0.83
Electrode Voltages	± 7.7 kV
Electrode Gap at Entrance	8.0 mm
Electrode Gap at Exit	6.0 mm
Fringe Field Effective Length	1.5 mm
Fringe Field Weighting Factor	1.0
Mapped Axial Bore Magnetic Field	MAP29_DIGI.ZFLD
Electric Field Representation	Analytic

Image System: Quartz glass scintillators were placed at the inflector exit, and one half turn after the inflector exit as shown in Figure 1. Beams were detected on the scintillators whose output was recorded with a TV camera [5], and saved to disk. The beam image centroids were later computed using the image analysis software Optimetric [13], and *Mathematica* [14].

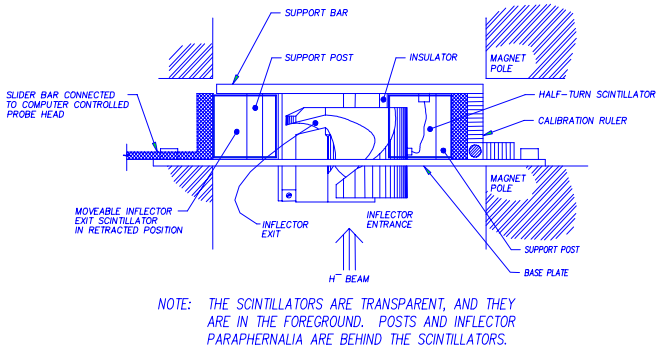

Figure 1: Experimental set-up

To view the scintillators through a vacuum tank port, an RF dee and its accompanying resonator stub were removed. The inflector exit scintillator is connected to a moveable, computer-controlled probe arm. It can be withdrawn to allow the beam to pass to the half-turn scintillator when desired. With the RF dee removed, the beam remains at 25 keV at the half-turn position.

3 Divergence Calculations

The shifts in beam centroids (Δx_{ex}, Δy_{ex}) at the exit, and (Δx_{ha}, Δy_{ha}) half-turn scintillators were recorded eight times for each experiment and then averaged. The standard error was computed for each averaged measurement.

The dipole magnetic field in the centre region is known, and, thus, the transport matrix R between the inflector exit and half-turn scintillators can be computed. Since magnetic mid-plane symmetry is maintained in the system, the off-diagonal sub-matrices of R are occupied by zeros. Consequently, the relationship shown in equation 1 can be established to compute the divergence components associated with the centroid shifts.

$$\begin{pmatrix} x'_{ex} \\ x'_{ha} \\ y'_{ex} \\ y'_{ha} \end{pmatrix} = \begin{pmatrix} -R_{11}^{ex,ha}/R_{12}^{ex,ha} & 1.0/R_{12}^{ex,ha} & 0.0 & 0.0 \\ R_{21}^{ex,ha} - R_{11}^{ex,ha} \cdot R_{22}^{ex,ha}/R_{12}^{ex,ha} & R_{22}^{ex,ha}/R_{12}^{ex,ha} & 0.0 & 0.0 \\ 0.0 & 0.0 & -R_{33}^{ex,ha}/R_{34}^{ex,ha} & 1.0/R_{34}^{ex,ha} \\ 0.0 & 0.0 & R_{43}^{ex,ha} - R_{33}^{ex,ha} \cdot R_{44}^{ex,ha}/R_{34}^{ex,ha} & R_{44}^{ex,ha}/R_{34}^{ex,ha} \end{pmatrix} \bullet \begin{pmatrix} x_{ex} \\ x_{ha} \\ y_{ex} \\ y_{ha} \end{pmatrix} \quad (1)$$

4 Inflector Potential Perturbations

In this experiment the inflector electrode potentials were adjusted while keeping all other injection line parameters at their nominal settings. The potentials were adjusted in concert about the nominal electrode voltages of ±7.7 kV, as shown in Figures 2 and 3, or independently, as shown in Figure 4.

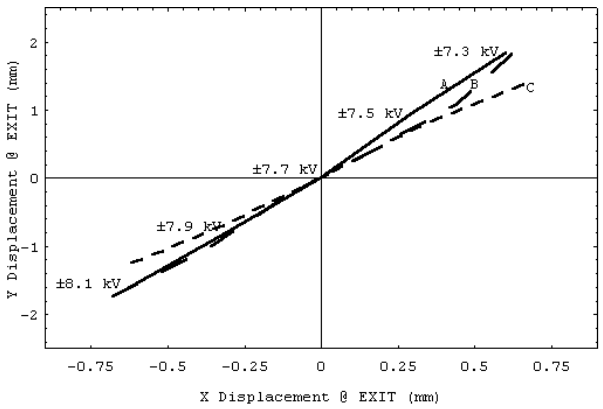

Figure 2: Central ray displacement at the inflector exit scintillator as a function of inflector electrode potential. (A) is measured data, (B) is CASINO data using electric field file INF_RELAX_14.DAT and magnet field file MAP29_DIGI.ZFLD, and (C) is CASINO data using an analytic electric field and magnetic field file MAP29_DIGI.ZFLD.

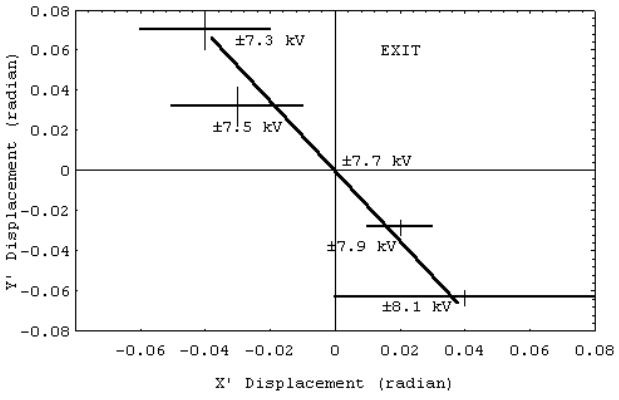

Figure 3: Central ray angular displacements at the inflector exit scintillator as a function of inflector electrode potential.

In Figure 2 data output from CASINO is overlaid for comparison. The match between the measured and modeled data is quite good. Casino results are not shown in Figure 4, as the program does not have an option for modeling asymmetric electrode potentials.

Figures 2 through 4 confirm that a wide range of beam position adjustments can be achieved by changing the electrode potentials, and Figure 5 shows how beam transmission to 1 MeV, during normal operation, varies as a function of changes in the electrode potentials.

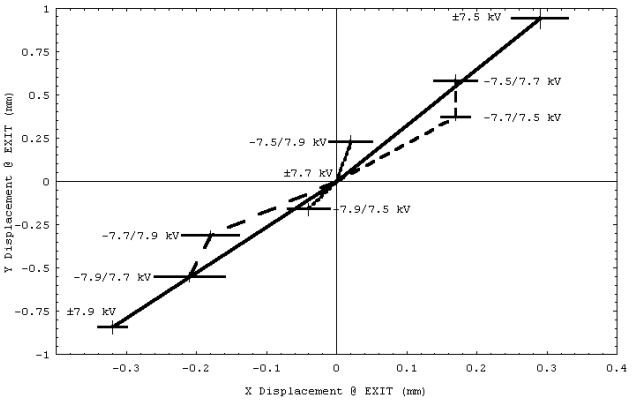

Figure 4: Central ray displacements at the inflector exit as a function of asymmetric inflector electrode potential settings.

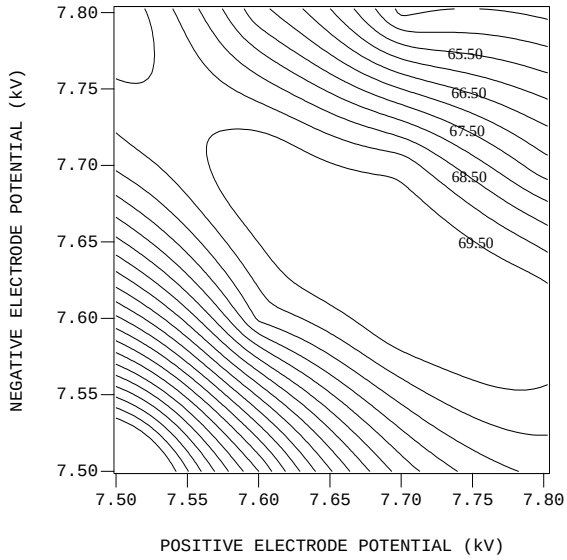

Figure 5: Beam current (micro-amperes) transmitted to the 1 MeV beamstop as a function of the inflector electrode potentials.

5 Beam Energy Perturbations

In this experiment only the injection energy was adjusted about its nominal setting while all other tuneable parameters were held constant at their nominal values. Figures 6 and 7 illustrate beam displacement at the inflector exit scintillator as a function of beam energy.

After analyzing the data from the inflector experiments it was determined that the inflector was slightly mis-positioned with respect to the median plane [5, 15]. To compensate for this the nominal injection line tune slightly mis-centres the beam at the inflector entrance to maximize transmission. Since the nominal beam is not injected along the injection axis, beams with different injection energies are steered differently by the nominal injection tune. The mis-centering at the inflector entrance was not known or even suspected *a priori*, and, since it was not measured, it was not possible to create a good model with CASINO. As a compromise the centroid locations at the inflector exit and half-turn scintillators are used to compute changes in electric and magnetic radii of curvature. As illustrated in Figure 6 the data calculated using equations $R = p/Bq$ and $A = 2Tg/\phi q$, where R is the magnetic radius of curvature, p is the momentum, B is the magnetic field, q is the charge, A is the electric bend radius, T is the injection energy, g is the electrode gap, and ϕ is the potential difference across the gap, compares favourably with the measured data.

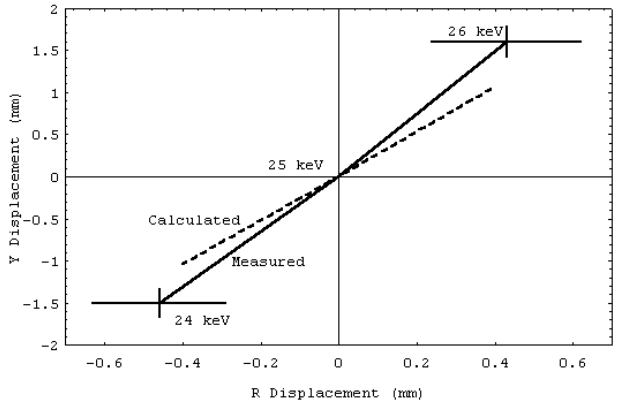

Figure 6: Changes in the Y displacement of the beam at the inflector exit (corresponds to changes in electric bend radius A) and the magnetic (R) radius of curvature of the injected beam as a function of the injected beam energy.

Figure 7: Changes in the angular displacement of the beam at the inflector exit as a function of the injected beam energy.

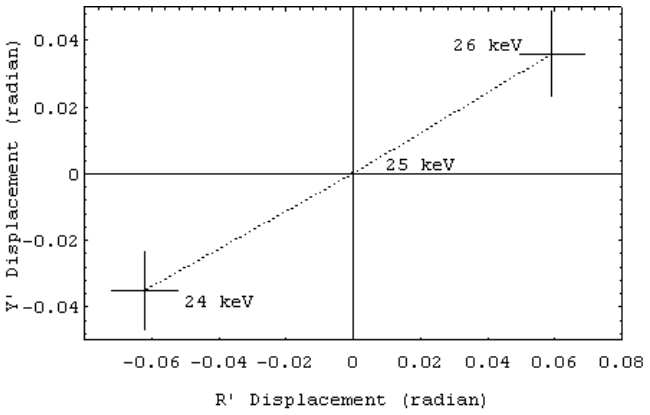

6 Magnetic Field Perturbations

In this series of measurements the only parameter varied from the nominal tune was the cyclotron's magnetic excitation current. Beam displacements for this case are shown in Figures 8 and 9. Again the mis-centering of the beam at the inflector entrance was a problem. By varying the cyclotron's excitation current the axial bore magnetic field upstream of the inflector entrance was also varied. Consequently changes in the strength of the solenoid axial bore field caused the mis-centred injected beam to also

change its inflector entrance coordinates. Since the entrance coordinates for each case were not measured, a meaningful CASINO model could not be created. Figure 8 compares CASINO data, which was computed using centred beams at the inflector entrance, to the measured data. As expected the measured and modeled data do not agree.

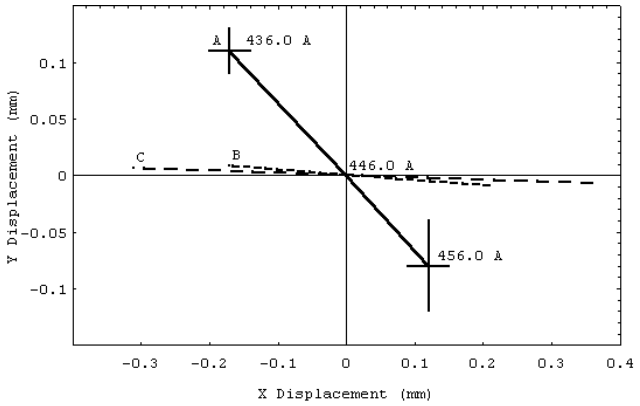

Figure 8: Beam displacement at the inflector exit as a function of the cyclotron excitation current. (A) is measured data, (B) is CASINO data using electric field file INF_RELAX_14.DAT and magnet field file MAP29_DIGI.ZFLD, and (C) is CASINO data using an analytic electric field and magnetic field file MAP29_DIGI.ZFLD.

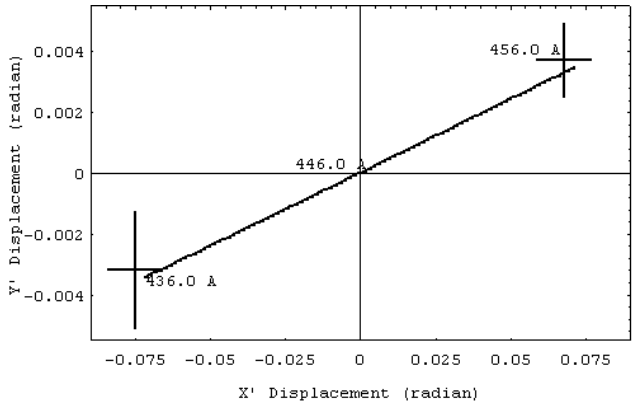

Figure 9: Angular displacement data at the inflector exit as a function of the cyclotron excitation current.

7 Conclusion

The measured data presented in this paper quantitatively illustrates beam displacement at the exit of a cyclotron's inflector as a function of adjustments in the inflector electrode potentials, the injected beam energy, and the cyclotron's excitation current. CASINO modeling of the data was found to be good for cases where accurate input data was available.

Beam mis-centering at the inflector entrance, discovered during these and other experiments [5, 15], was unexpected as beam transmission for the nominal tune was very high (14% to 1 MeV) and beam spill on collimators was quite low. The detailed nature of these experiments facilitated the discovery and rectification of the mis-centring problem.

Although full modeling comparisons were not possible for all experiments discussed, the novel experimental techniques described in this paper produced measured data useful for practical injection optimization.

Acknowledgements

This paper is based on a Doctoral thesis at the University of B.C.. The guidance of Dr. E. Auld, the financial support of Ebco Technologies Inc., TRIUMF and the Science Council of B.C. is gratefully acknowledged. The authors would also like to thank all the technical staff at Ebco Technologies Inc. and at TRIUMF for assisting with the manufacture of the equipment, and K. Dehnel for drafting Figure 1.

References

[1] B.F. Milton *et al*, "A 30 MeV H^- Cyclotron for Radioisotope Production", *Proc. 12th Int'l Conf. on Cyclotrons and their Applications*, pp. 145-148, Berlin, 1989.

[2] K. Erdman *et al*, "Operation of the TR30 Industrial Cyclotron", *Proc. IEEE Part. Acc. Conf.*, Vol. 3, pp. 1733-1734, Washington, 1993.

[3] R.E. Laxdal *et al*, "Beam Measurements on a Small Commercial Cyclotron", *Proc. 4th European Part. Acc. Conf.*, Vol. 1, pp. 545-547, London, 1994.

[4] K.L. Erdman *et al*, "Initial Operation of the Sherbrooke Ebco 19 MeV Cyclotron", *these proceedings.*

[5] M.P. Dehnel *et al*, "The Experimental Characterization of a Compact H^- Cyclotron's Spiral Inflector", *Nucl. Instrum. & Methods in Phys. Research A*, Vol. 396, pp. 35-44, 1997.

[6] B.F. Milton, "Central Region Specification – Revision 1", TRIUMF design note, TRI-DN-19, rev. 1, 1989.

[7] R.J. Balden *et al*, "Aspects of Phase Space Dynamics in Spiral Inflectors", *Proc. 12th Int'l Conf. on Cyclotrons and their Applications*, pp. 435-438, Berlin, 1989.

[8] R. Baartman, "Intensity Limitations in Compact H^- Cyclotrons", *Proc. 14th Int'l Conf. on Cyclotrons and their Applications*, pp. 440-445, Capetown, 1995.

[9] T. Kuo *et al*, "On the Development of 2 mA RF H^- Beams for Compact Cyclotrons", *Proc. 14th Int'l Conf. on Cyclotrons and their Applications"*, Capetown, 1995.

[10] B.F. Milton *et al*, "CASINO: Calculation of Spiral Inflector Orbits – User's Guide and Reference Manual", TRIUMF design note TRI-DN-89-19, 1989.

[11] W. Kleeven *et al*, "Status and Results from the TR30 Cyclotron Centre Region Model", *Proc. 2nd European Part. Acc. Conf.*, Vol. 1, pp. 434-436, Nice, 1990.

[12] M.P. Dehnel, Ph.D. Thesis, University of British Columbia, Vancouver, 1995.

[13] OPTIMETRIC™, BioScan® Incorporated, 170 West Dayton, Suite 204, Edmonds, WA, USA 98020.

[14] *Mathematica*® Version 2.2, Wolfram Research Inc., 100 Trade Center Drive, Champaign, IL, USA 61821-9910.

[15] M.P. Dehnel *et al*, "Injection System Design and Tests for the TR13 Cyclotron", *Proc. 4th European Part. Acc. Conf.*, Vol. 3, pp. 2367-2369, London, 1994.